ICOLD Symposium on Sustainable Development of Dams and River Basins, 24th - 27th February, 2021, New Delhi

PROTOTYPE OBSERVATIONS AND NUMERICAL MODELLING OF GEYSERS FROM A BOTTOM OUTLET

J. YANG, P.H. TENG AND S.C. LI
Civil & Architectural Engineering, Royal Institute of Technology (KTH), Stockholm, Sweden

F. MIDBÖE
HydroTerra Ingenjörer AB, Karlstad, Sweden

M. BERGMAN AND L. ORMANN
Fortum Sverige AB, Karlstad, Sweden

ABSTRACT

The bottom outlet in question comprises a bulkhead gate, a vertical shaft, a horizontal tunnel and a submerged exit in the tailwater. Field tests show that the gate outflow at partial openings entrains air into the tunnel which leads to blowouts at the exit. CFD modeling is performed, with the purpose to understand the phenomenon and estimate the amount of trapped air. The gate is instantaneously opened to a designated position. Three gate opening heights, 0.45, 0.80 and 5.00 m (full opening), are modelled. The simulations show that, due to the impact of the gate outflow, surge oscillations occur in the shaft-tunnel-tailwater system; the surge amplitude descends with time. The air entrained in the shaft enters the tunnel and forms air pockets that follow the tunnel flow downstream. The air pockets travel along the roof of the tunnel and may coalesce and break up. At the 0.45-m opening, the blowouts in the model exhibit almost the same frequency (28–29 s) as observed in the field tests (~30 s). At the 0.80-m opening, more air is entrained in the shaft; after the first major blowout, the air is released in form of small blowouts, mostly at a 7–12 s frequency. The blowouts are found to be associated with small gate openings. At the full opening, air ceases to enter the tunnel and water is discharged without air entrainment and blowouts.

1. LAYOUT OF BOTTOM OUTLET

The hydropower scheme in question is situated in South Sweden. The facility comprises two main embankment dams, both belonging to hazard Class B according to the Swedish dam-safety legislation. Their crest lengths are 1800 and 2200 m; the maximum structural heights are 25 and 22 m, respectively. The full reservoir retention level (FRRL) is +349.00 m, corresponding to which the water-surface area is 16.30 km^2. The legal reservoir amplitude is 19.00 m.

The pumped storage hydropower plant is located underground in bedrock. The plant intake is placed in the reservoir bottom. From the reservoir, a more than 6000-m rock tunnel, followed by a 250-m penstock, conveys the water to the power house. The 1170 m long tailrace tunnel discharges then the water into the river.

The dam has one bottom outlet. Above it, there is also a surface opening controlled with concrete stop-logs, with a discharge capacity of 24 m^3/s. However, it is seldom used. It is the bottom outlet that is usually used to discharge flood waters. The outlet includes an intake tower with a gate shaft, a submerged bulkhead gate, a 90° double-miter bend, a horizontal conduit and a tailwater exit that is submerged even at low flow discharges. The outlet and the surface opening share the vertical shaft and the downstream waterway. Figures 1 and 2 show its longitudinal layout and the intake tower and tunnel exit (when emptied of water).

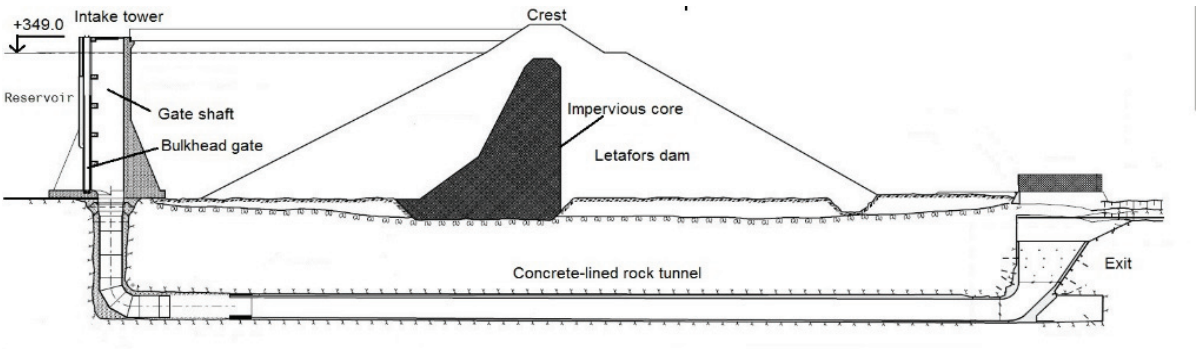

Figure 1 : Bottom outlet examined, longitudinal profile showing the gate opening, gate shaft, bend, conduit and exit. The conduit is horizontal.

Figure 2 : Bottom outlet, with the intake tower in front of the embankment dam and the exit in the tailwater. The right photo shows the exit during a planned maintenance when the outlet was emptied of water.

The bulkhead gate is 3.05 m wide, its full opening height is 5.00 m. The gate threshold elevation is +332.80 m. The gate shaft, open to the atmosphere, is placed immediately downstream of the gate. The 90° mitred bend is formed with a circular steel pipe (diameter 2.55 m), followed by a short section of circular concrete lining of the same diameter. The major part of the conduit is about 90 m long and has a rectangular cross-section of 2.55 m wide and 2.55 m high, with rounded corners (Figure 3). There is an 8-m streamlined transition between the two cross-section types. The bottom elevation of the conduit is the same throughout the conduit, i.e. +321.40 m (27.60 m below the FRRL). The typical tailwater level is around +330.00 m.

Figure 3 : Horizontal conduit – a short section of circular conduit (diameter 2.55 m) downstream of the bend (left); the major rectangular conduit (2.55 m in width, 2.55 m in height) with rounded corners running to the exit (right).

2. FIELD TESTS AND GEYSERS

During operations of the bulkhead gate, blowouts, or geysers as usually called, occurred at the tunnel exit (Figure 4). This was obviously due to the entrained air in the gate shaft that was carried into the tunnel. No de-aeration structure existed along the tunnel. Previously, blow-outs were observed at gate openings around 0.30 m (no opening gauge was installed). The frequency of major blowouts was about 30 s. With a gauge, new field tests were conducted at 0.40–0.50 m gate openings. The frequency of the major blowouts was more or less the same, still every 30 s.

The major factors involved include discharge capacity, flow fluctuations and amount of entrained air in the tunnel. With the aim to understand the phenomenon, CFD simulations are performed. The main purposes of the study include the following aspects. (1) to evaluate if CFD can reproduce the hydraulic phenomenon observed in the field tests; (2)

to identify, with CFD modelling, major scenarios at different gate openings. (3) to estimate volumes of the trapped air as it is otherwise difficult to quantify it by other means and (4) to predict the frequency of air blowouts downstream at various gate openings.

Figure 4 : Sequential blowouts at the exit, occurring at relatively small gate openings, 0.30–0.50 m.

3. NUMERICAL SIMULATIONS

A 3D numerical model of water-air flows is set up for the outlet. The commonly used VOF method is adopted for the prediction, in which a set of momentum equations are shared by the two fluids and the VOF is calculated in each cell throughout the domain. Water is usually treated as the primary phase and the air as the secondary one (α_w = fraction of water and α_a = fraction of air; for a given cell $\alpha_w + \alpha_a = 1.0$). The method uses a surface-tracking technique applied to a fixed Eulerian mesh (Hirt and Nichols 1981, ANSYS 2011). The Realizable k-ε turbulence model proves to be superior to other turbulence models. It is more suitable to represent the free-surface turbulent flows with air entrainment (Zhang et al. 2011, Jothiprakash et al. 2015, Teng et al. 2016).

The computational domain and grid are shown in Figure 6(a). The modelled reservoir area covers 50 m upstream of the gate. A sufficiently large area is included for the tailwater. The total number of cells adopted in the simulations amounts to 960 000. A higher mesh density is given to areas around the gate, the lower part of the shaft, the upper part along the conduit and the conduit exit where air pockets start to rise. CFD modelling must guarantee grid-independent solutions. The ASME editorial policy statement provides guidelines for estimation of discretization errors of CFD simulations, in which the grid convergence index (GCI) method helps check the grid convergence (Celik *et al.* 2008). Usually, a relatively coarse grid is first generated. It is then refined, both globally and locally, to satisfy the criterion.

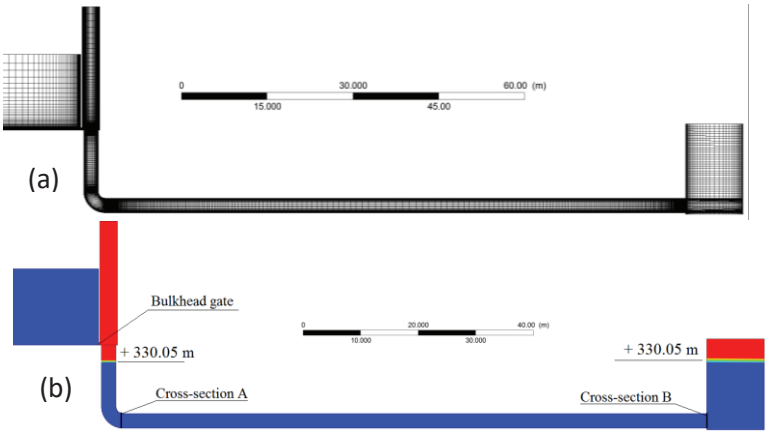

Figure 6 : (a) Numerical grid, with higher density in areas of air-water mixing and presence of air pockets; (b) Initial conditions of static water level in the conduit and denotation of cross-sections A and B.

The near-wall grids should be fine enough to reasonably reproduce the boundary layer flow. A dimensionless parameter of wall distance is usually defined, $y^+ = u_\tau d/\upsilon$, where υ = water kinematic viscosity, u_τ = shear velocity and d = centroid distance of the first cell to wall boundaries. The y^+ value should be between 10 and 100. The y^+ values in the study is in the range of 10−40. The Enhanced Wall Function is also activated for the viscous layer.

The vertical boundaries in the reservoir include two parts. The water part is given as pressure inlet with a hydrostatic pressure. The air part above the water surface, together with the upper reservoir boundary and the shaft's upper end, is specified as pressure inlet with the atmospheric pressure, allowing free air flow across it. The tailrace water level is specified as pressure outlet with hydrostatic pressure. Figure 6(b) shows the boundary conditions. The reservoir and tailwater levels are related to each other, set at +346.00 and +330.05 m, respectively.

In the simulations, the bulkhead gate is simultaneously opened to a designated height, thus generating a transient flow of water and air in the outlet. For each time step, a fully implicit numerical scheme is used, in which the iterative convergence is checked. There is no stability criterion that governs the choice of time steps. It is usually set at least one order of magnitude smaller than the smallest time constant of the system. A common way to judge its choice is to count the number of iterations to a converged solution. 5–10 iterations per time step are ideal. The iterative convergence is achieved with a decrease by at least three orders of magnitude in the normalized residuals. In summary, the numerical setup follows the best practice guidelines for two-phase flow modeling (ERCOFTAC 2000, 2008).

4. AIR ENTRAINMENT AND TRANSPORT

The field tests, as well as operation experiences, indicate that the amount of entrained air is associated with gate openings and small openings draw special attention. The gate is instantaneously opened to a designated position. Three cases are simulated, i.e. a = 0.45, 0.80 and 5.00 m, where a = gate opening height. Two cross sections, A and B, are chosen to monitor the flow. Section A is at the beginning of the horizontal conduit and B is at its end (Figure 6).

4.1 Flow case a = 0.45 m

For case a = 0.45 m, Figure 7 plots the sequential pictures of VOF from time t = 2.8 s to 72.5 s at which the simulation ends. Blue (α_w = 1.0) and red (α_a = 1.0) colors denote the water and air phases, respectively. The side views are cut through the center plane of the outlet. From Figure 7e (t = 25.0 s), even the top views from above the conduit are shown.

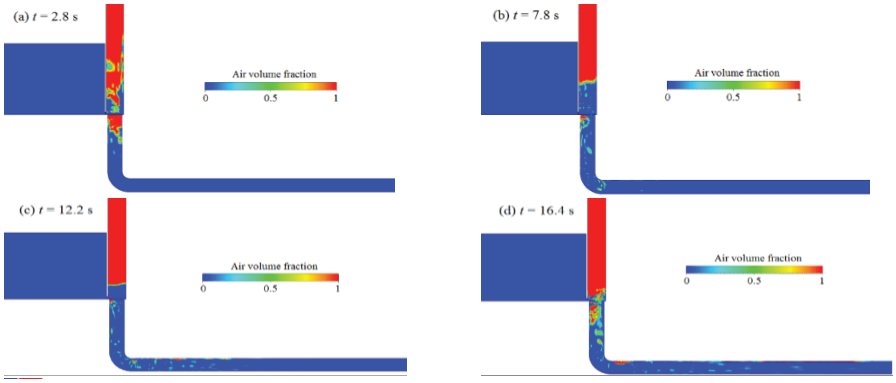

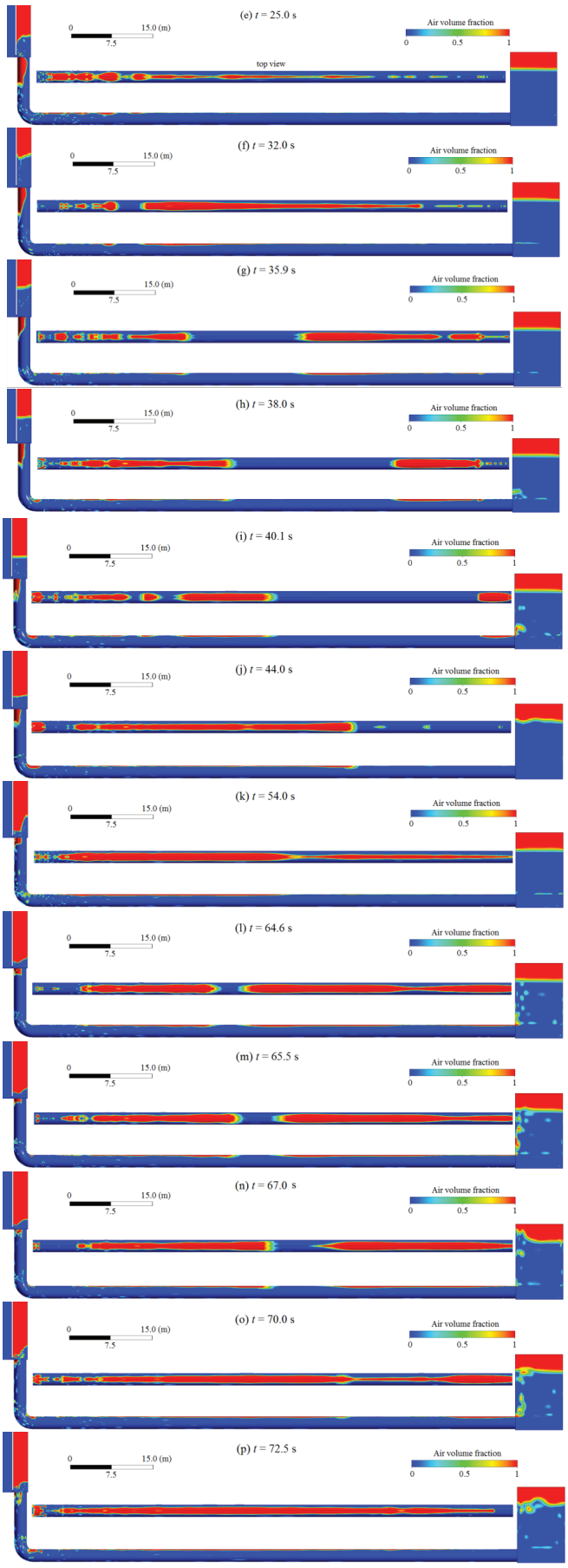

Figure 7 : Flow case at a = 0.45 m – a sequence of VOF plots showing entrainment, transport and detrainment of air in the outlet. The reservoir and tailwater levels are at +346.00 and +330.05 m.

Let Q_w (m³/s) denote water-flow rate of the waterway. Figure 8a illustrates the change of Q_w below the bulkhead gate and the dynamic pressure h (m water column) that acts upon the gate sill in the shaft. After the gate is opened ($0 < t < 1$ s, it is free outflow, $Q_w \approx 14.5$ m³/s. The gate outflow is affected by the pressure change immediately downstream of the gate. After $t > 65$ s, the shaft water level becomes relatively stable and the outflow is almost free; Q_w fluctuates somewhat about 14 m³/s, slightly affected by the water in the shaft.

Figure 8b shows the Q_w variation at cross-sections A and B. Q_w features both large oscillations and small add-on fluctuations. The oscillational frequency is probably related to the natural frequencies of the outlet, as the flow in the shaft-conduit-tailwater system is paralleled to surge oscillations in a U-tube. The oscillational amplitude declines with time. The fluctuations are ascribable to the changes in dynamic pressure in the shaft. When $t > 70$ s, the conduit flow approaches a relatively stable level; its averaged value is nearly the same as the gate outflow rate, $Q_w \approx 14$ m³/s.

Figure 8c shows the air flow rates (Q_a, m³/s) at sections A and B. From $t = 5$ s, the air continually flows into the conduit from section A. Up to $t = 19$ s, there is no air present at section B. The first peak appears at $t \approx 40$ s. It means that a large air pocket blows out in the tailwater. The air movement velocity is dependent on the water flow velocity in the conduit. The second large air pocket appears at $t = 66$ s; its release lasts 5 s. The time interval between the first and second pockets is $T = 28$–29 s.

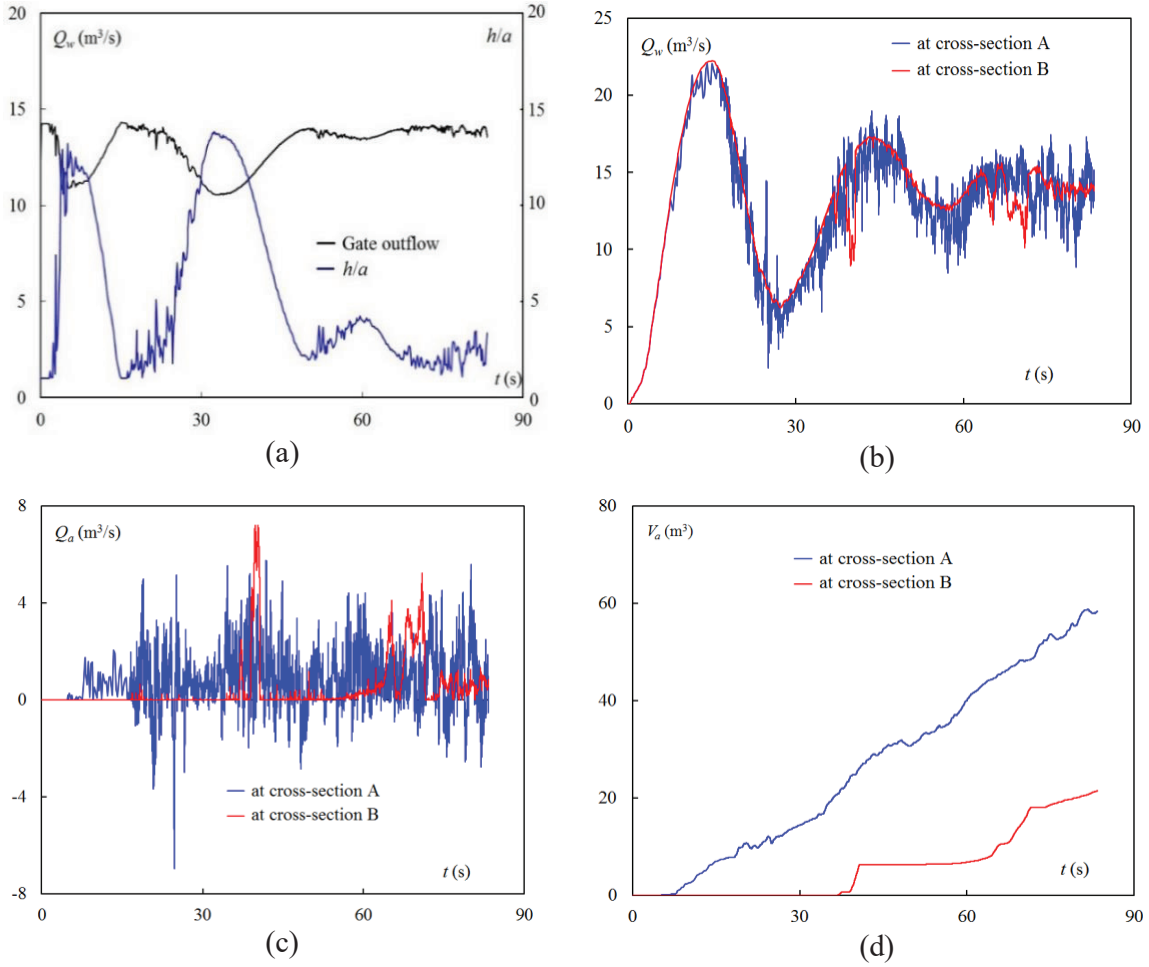

Figure 8 : Case $a = 0.45$ m – (a) change of Q_w at the gate and h/a with time; (b), (c) and (d) changes of Q_w, Q_a and V_a at cross-sections A and B.

Figure 8d shows the accumulations of air amount (V_a, m³) into and out of the conduit. From $t = 5$ s, air continues to be transported down the vertical shaft and into the conduit through section A and V_a increases almost linearly with time. At $t = 36$ s, the long air bubble starts to blow out through section B. As the conduit is about 100 m long, the storage of air is significant.

4.2 Flow case a = 0.80 m

For case $a = 0.80$ m, Figure 9 shows the corresponding results. The gated outflow becomes relatively stable and the opening is submerged ($h/a > 5$) when $t > 40$ s; Q_w at the gate fluctuates about 24 m³/s (Figure 9a). For the flow in the conduit, it takes however much longer time to stabilize, which is partially attributed to the air entrainment (Figure 9b).

For air bubbles to reach section B, it takes shorter time than in the a = 0.45 m case, which is due to higher flow velocity. The first major blowout occurs at $t \approx 33$ s, followed by a series of minor ones (Figure 9c). This is in line with the field observations roughly at the same opening. The minor blowouts occur continuously, with much lower peaks than the first one and mostly at a frequency of 7–12 s. Obviously, more air is entrained at a = 0.80 m than at a = 0.45 m (Figure 9d).

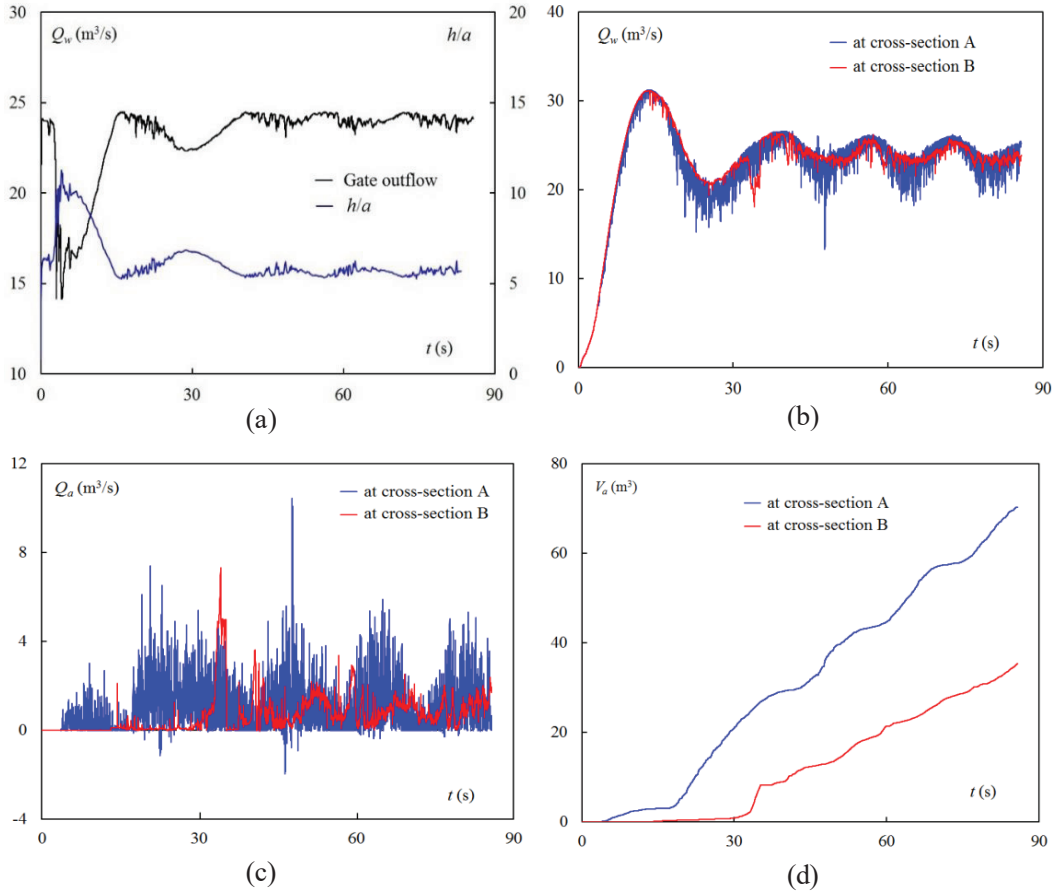

Figure 9 : Flow case a = 0.80 m – (a) change of Q_w at the gate and h/a with time; (b), (c) and (d) changes of Q_w, Q_a and V_a at cross-sections A and B.

4.3 Flow case a = 5.00 m

For the full gate opening (a = 5.00 m), Figure 10 illustrates the results of Q_a and V_a at cross-sections A and B. As the initial shaft water stage is 2.75 m below the outlet sill elevation, the outflow jet plunges into the water and mixing occurs in the shaft following the sudden opening of the gate. A major blowout takes place at t = 15 s. As the shaft water level rises, the gate opening becomes completely submerged and air entrainment ceases. At the steady state, the submerged outflow amounts to 72 m³/s. The shaft water level stabilizes at +345.1 m, i.e. 7.3 m above the upper edge (+337.80 m) of the gate opening and 0.9 m below the reservoir level (+346.00 m). It can be stated that the outlet operates without air entrainment at large gate openings.

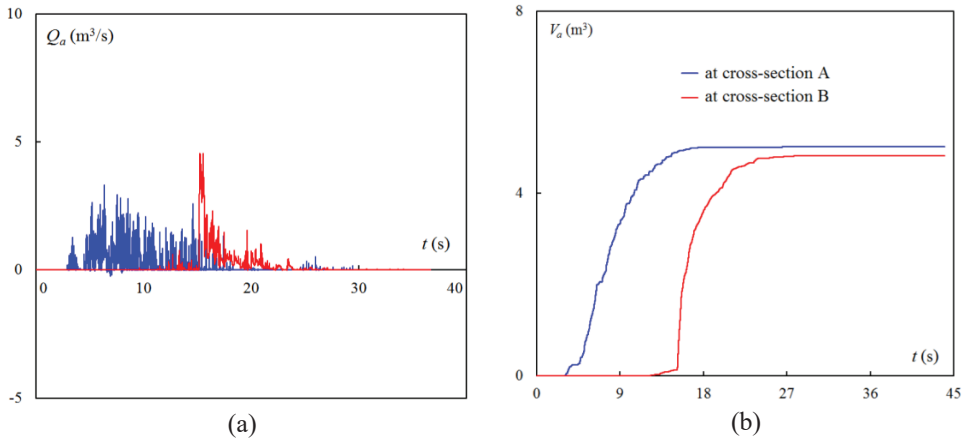

Figure 10 : Flow case a = 5.00 m (full opening) – changes of Q_a and V_a at cross-sections A and B.

5. CONCLUSIONS

Operations of the bottom outlet in question led to air entrainment in the gate shaft and transport of air pockets in the conduit, which was evidenced from the blowouts in the river. This gave rise to undesirable flow fluctuations in the system. Investigations have been made, with the purpose to determine the actual outlet discharge capacity at different gate openings, to better understand the influence that the discharge exerts on the structure, to propose necessary operation restrictions and to provide basis for countermeasures to guarantee safe outlet discharge.

With the field observations in background, CFD modelling is performed to help understand the flow conditions. A suddenly opened gate is modeled, which differs from the reality. However, it is the steady state that is of concern for real gate operation. The phenomenon is seemingly related the gate opening size, giving rise to different degrees of water-air mixing and air entrainment. With the opening changing from 0.45 to 0.80 m, the flow rate and the energy of the plunging water increase. As a result, the jet penetrates deeper in the gate shaft, implying that it is possible that more air is "pushed" into the tunnel. However, a further increase in gate opening leads to a higher shaft level and submergence, which implies that shaft water may enclose the gate opening and air entrainment ceases to occur. Further CFD simulations of flow cases between the 1.00 and 5.00 m gate openings would provide more information about the degree of air entrainment and give insight into overall picture of the outlet.

ACKNOWLEDGEMENTS

The study is funded by Fortum Sverige AB and also by Swedish Hydropower Centre (SVC). It falls within the frame of two SVC research projects entitled *Two-phase flow modeling: Evaluations and simulations for safer spillway discharge* (VKU 14126) and *Investigation of air blowout (geyser) from bottom outlets for safe operation* (VKU 14137). The KTH authors are indebted to Professor Anders Ansell of KTH Civil & Architectural Engineering for co-ordinations of diverse issues and to Ms. Emma Hagner and Dr. Bertil Wahlund of SVC for project administration.

REFERENCES

ANSYS Inc. 2011. *ANSYS FLUENT Theory Guide*. Canonsburg: ANSYS Inc.

Blocken, B. and Gualtieri, C. 2012. Ten iterative steps for model development and evaluation applied to Computational Fluid Dynamics for Environmental Fluid Mechanics. *Environmental Modeling Software*. 33:1–22.

Falvey, H.T. 1980. *Air-water flow in hydraulic structures. Engineering Monograph 41*. Denver: United States Department of the Interior, Bureau of Reclamation.

Celik, I.B., Ghia, U. and Roache, P.J. 2008. Procedure for estimation and reporting of uncertainty due to discretization in CFD applications. *Trans ASME Journal of Fluids Engineering*, 130:7.

ERCOFTAC 2000. *Best Practice Guidelines, Industrial Computational Fluid Dynamics of Single-Phase Flows*. London: ERCOFTAC.

ERCOFTAC 2008. *Best Practice Guidelines, Computational Fluid Dynamics of Dispersed Multi-Phase Flows*. London: ERCOFTAC.

Hirt, C.W. and Nichols, B.D. 1981. Volume of fluid (VOF) method for the dynamics of free boundaries. *Journal of computational physics*, 39(1), 201–225.

Jothiprakash, V., Bhosekar, V.V. and Deolalikar, P.B. 2015. Flow characteristics of orifice spillway aerator: numerical model studies. *ISH Journal of Hydraulic Engineering*, 21(2), 216–230.

Khatsuria, R.M. 2005. *Hydraulics of spillways and energy dissipators*. New York: Marcel Dekker.

Liu, T. & Yang, J. 2014. Three-dimensional computations of water-air flow in a bottom spillway during gate opening. *Engineering Applications of Computational Fluid Mechanics*, 8(1), 104–115.

Teng, P., Yang, J. and Pfister, M. 2016. Studies of two-phase flow at a chute aerator with experiments and CFD modelling. *Modelling and Simulation in Engineering*, Volume 2016, Article ID 4729128.

Yang, J., Larsson, J. and Nilsson, C.-O. 2016. Re-commissioning Storfinnforsen's bottom outlet after over 60 years' idling. In *Proceedings of ICOLD 2016 Annual Symposium*, Johannesburg: ICOLD.

Zhang, J.M., Chen, J.G. and Xu, W.L. 2011. Three-dimensional numerical simulation of aerated flows downstream sudden fall aerator expansion in a tunnel. *Journal of Hydrodynamics*, 23(1), 71–80.